# Supporting Information for "Absolute Centroid Location of Submarine Earthquakes from 3D Waveform Modeling of Water Reverberations"

Jorge C. Castellanos[1], Zhongwen Zhan[1], and Wenbo Wu[1]

[1]Seismological Laboratory, Department of Earth and Planetary Sciences, Caltech, Pasadena, California, USA.

**Contents of this file**

1. Text S1 to S2

2. Figures S1 to S13

**Additional Supporting Information (Files uploaded separately)**

1. Caption for Movie S1

**Introduction**

This section adds a number of additional details on the specifics of the 3D hybrid simulations. Some aspects of the data used in this study are also described.

**Text S1.**

The extent of the SEM model that was used to compute all of the 3D wavefields is 10°x10°x80 km. Such model is meshed using the parameters of NX=320 (Longitude), NY=320 (Latitude) and NZ=24 (vertical), which allows us to resolve a minimum period of about 2 s. Stacey absorbing boundaries are applied on the bottom and each of the four

sides. We use 400 CPU processors and each simulation takes about 3 hours. Figure S2 shows a series of synthetic tests using different sized SEM boxes.

**Text S2.**

To ensure that the pair of events used to conduct the analysis presented in Figure 12 are separated by similar distances, we measured the time shifts between their Rayleigh wave packets at a full azimuth range, and estimated their approximate intersource distances assuming a surface wave velocity of 3.7 km/s. This analysis was performed within the 30 to 80 s period band, where the group and phase velocities are mostly flat and have little dispersion sensitivity (e.g. Cleveland and Ammon, 2013). Figures S12-13 shows the analysis for the two pair of events.

**Movie S1.**

2D finite-difference simulation of a 5 km depth strike-slip source in a two-domain (i.e. fluid and solid) velocity model with a flat ocean bottom.

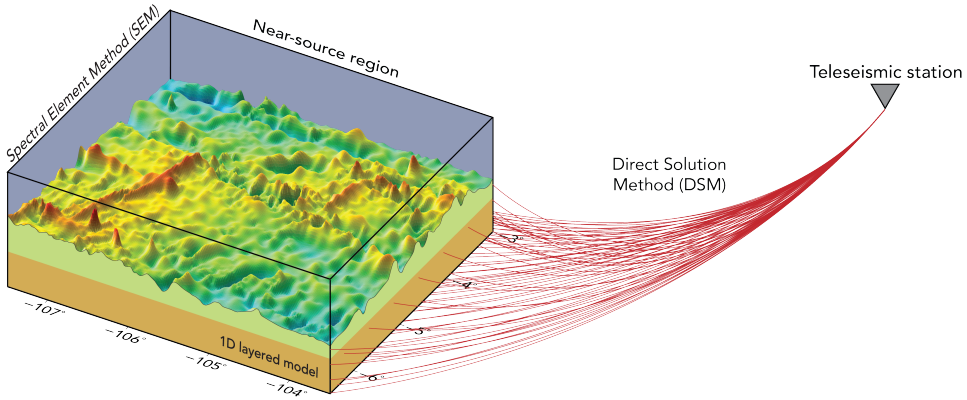


**Figure S1.** Schematic cartoon to illustrate the configuration of SEM-DSM coupling. The method uses the Spectral Element Method (SEM) to compute a complex 3D wavefield in the source region and then propagates that wavefield to large epicentral distances using the Direct Solution Method (DSM).

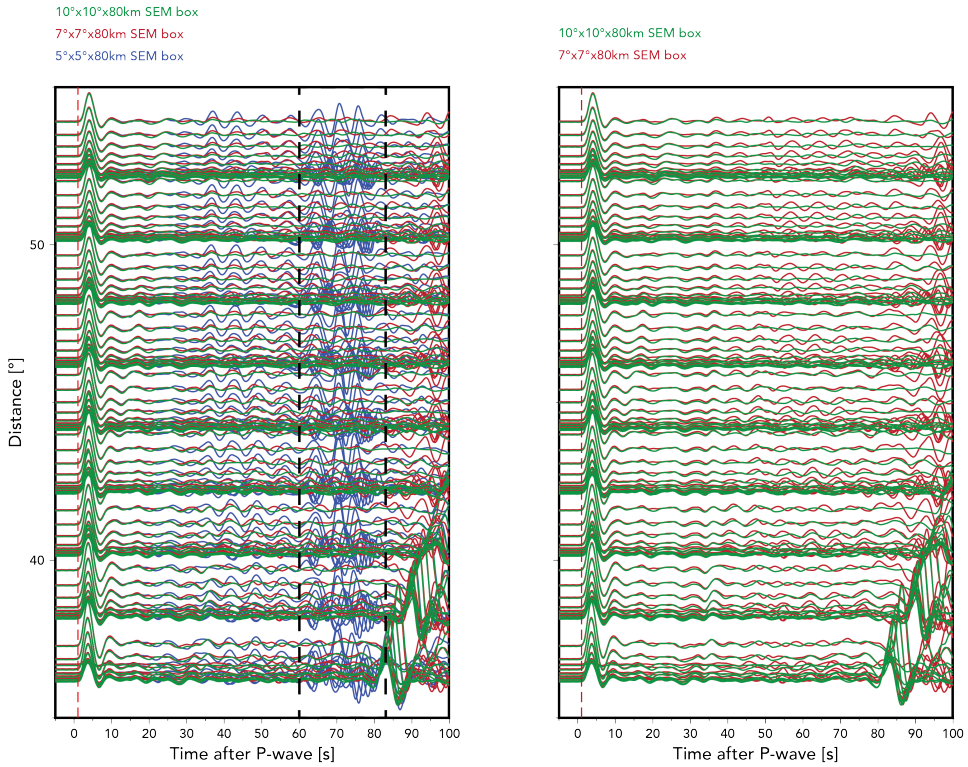


**Figure S2.** Synthetic waveforms computed for a flat ocean model using different-sized SEM boxes. The black dashed box in the left panel encloses some spurious arrivals that are product of artificial reflections from the boundaries of the box. These errors decrease with the horizontal dimensions of the SEM domain. The source is a 5 km depth strike slip source.

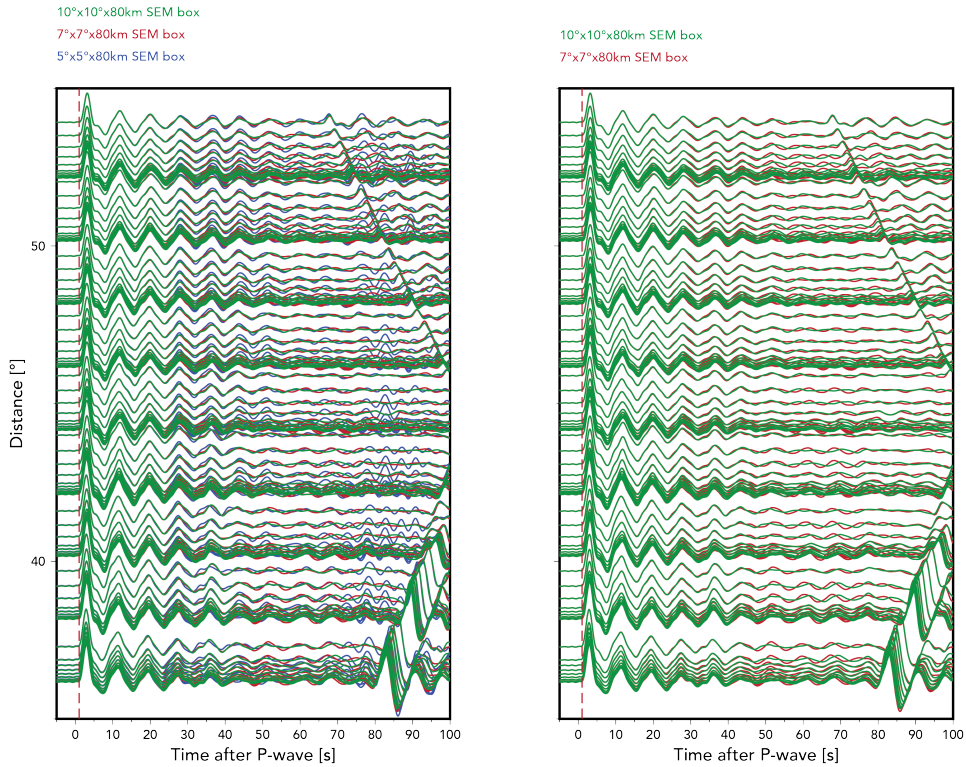


**Figure S2.** Synthetic waveforms computed for a flat ocean model using different-sized SEM boxes. The source is a 5 km depth explosion. Note how the boundaries effects are smaller than those that are observed for a double-couple source (Figure 2A).

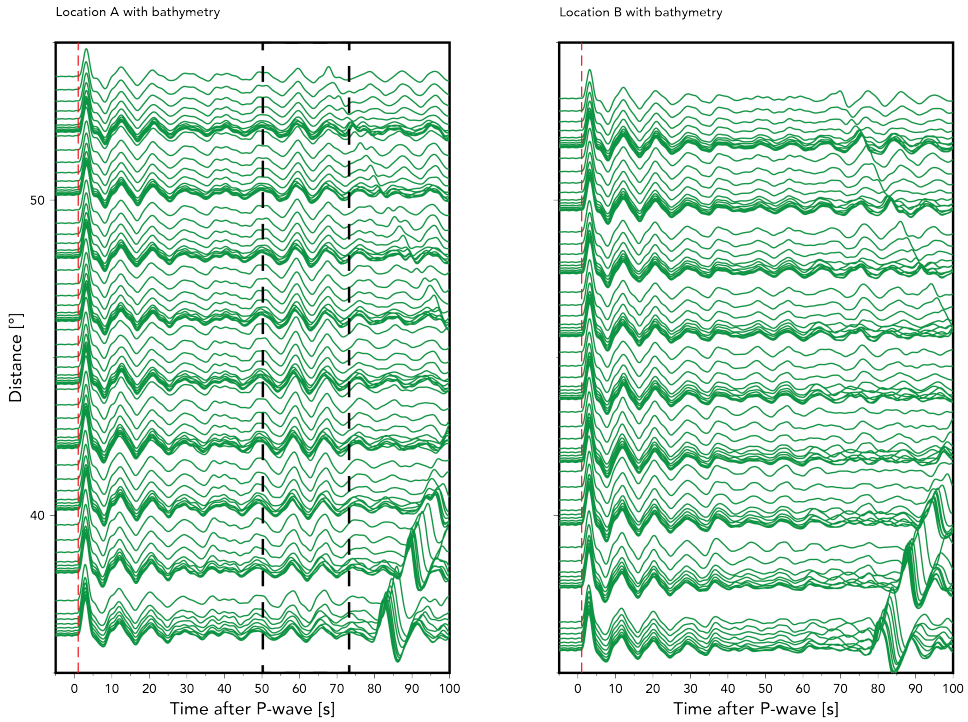


**Figure S2.** Synthetic waveforms of two different localized strike slip sources computed for a realistic ocean model. The size of the SEM box is 10°x10°x80 km and the depth of the sources is 5 km. Based on the analysis made with Figures 2AB, the coda waves in the black dashed box of the left panel are likely to be real and not an artifact of the simulation.

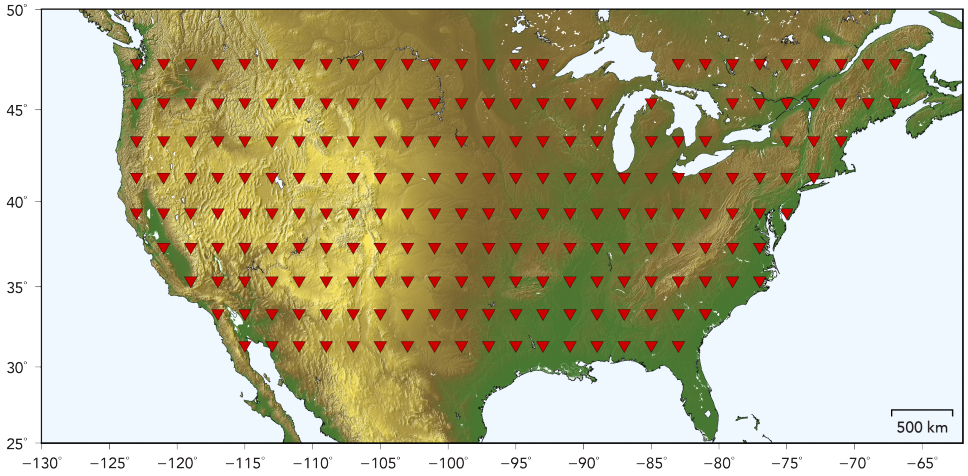


**Figure S3.** 207 station array used to perform the source-side beamforming presented in Figure 6 of the main text.

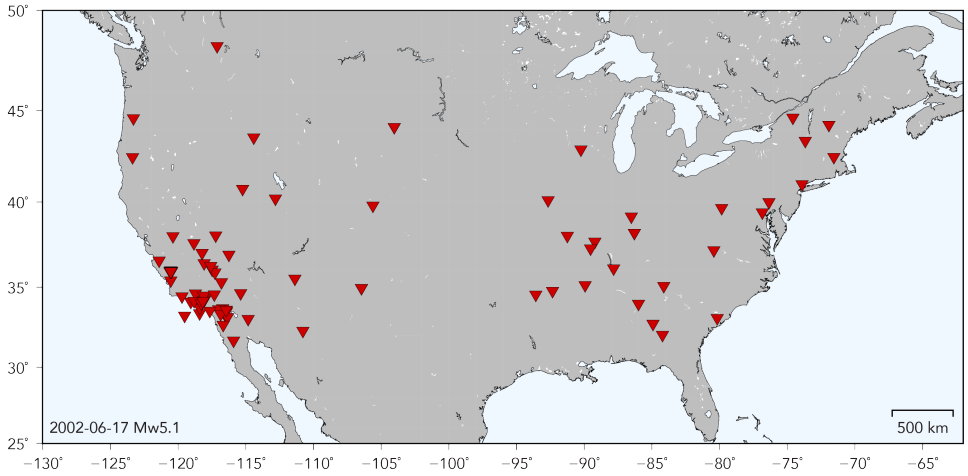


**Figure S4.** Distribution of seismic stations where the 2002 Mw5.1 event was simulated. The station selection was based on the quality of the earthquake recordings.

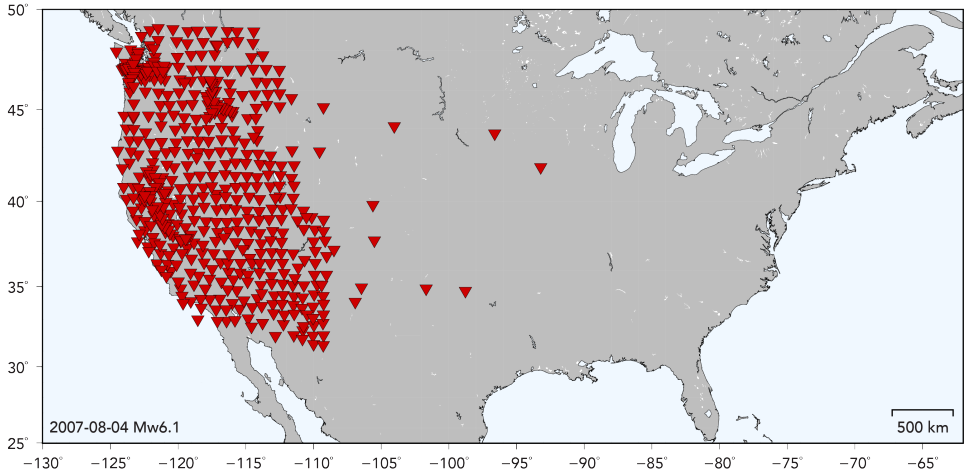


**Figure S5.** Distribution of seismic stations where the 2007 Mw6.1 event was simulated. The station selection was based on the quality of the earthquake recordings.

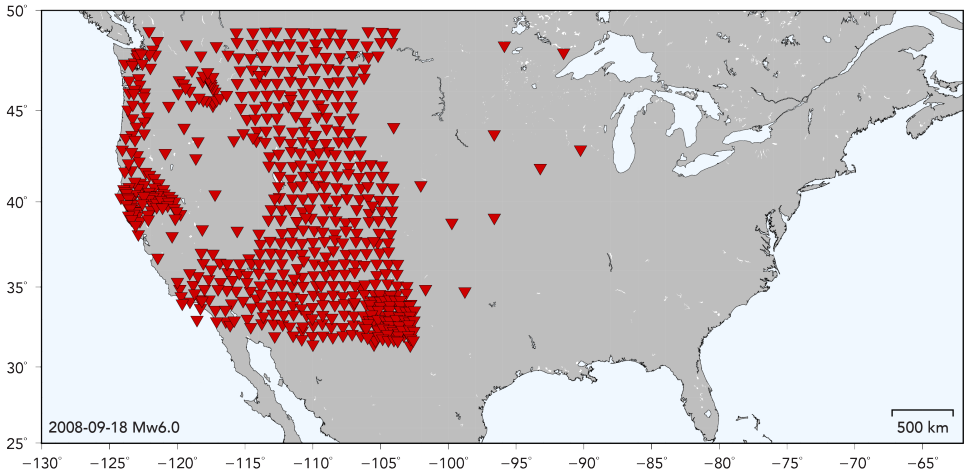


**Figure S6.** Distribution of seismic stations where the 2008 Mw6.0 event was simulated. The station selection was based on the quality of the earthquake recordings.

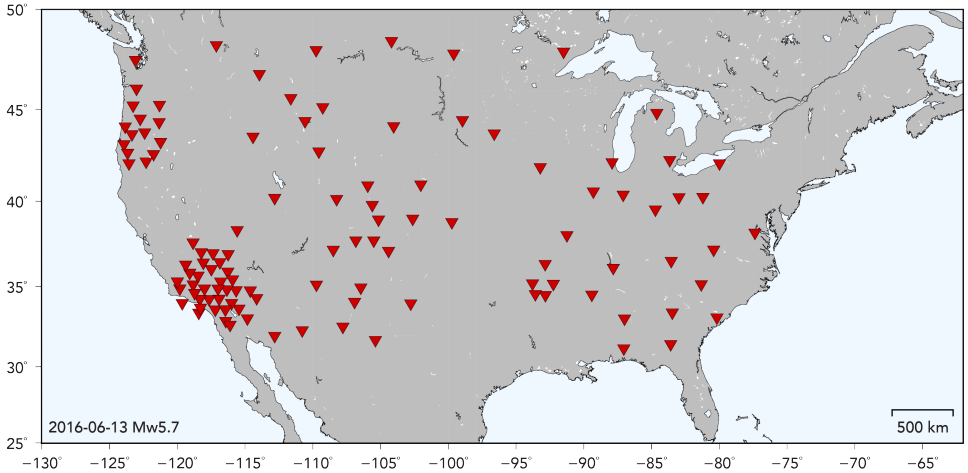


**Figure S7.** Distribution of seismic stations where the 2016 Mw5.7 event was simulated. The station selection was based on the quality of the earthquake recordings.

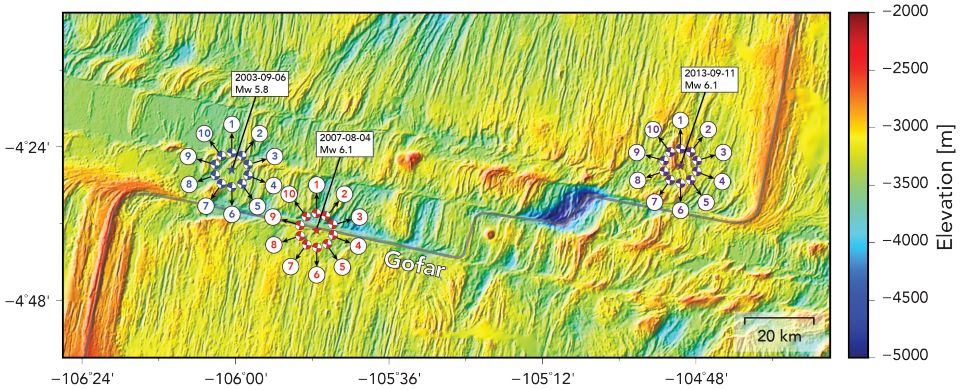


**Figure S8.** Distribution of seismic sources used to test the sensitivity of the wavefield to horizontal location for 3 different events. The waveform modeling results for each event are presented in Figure S9-11.

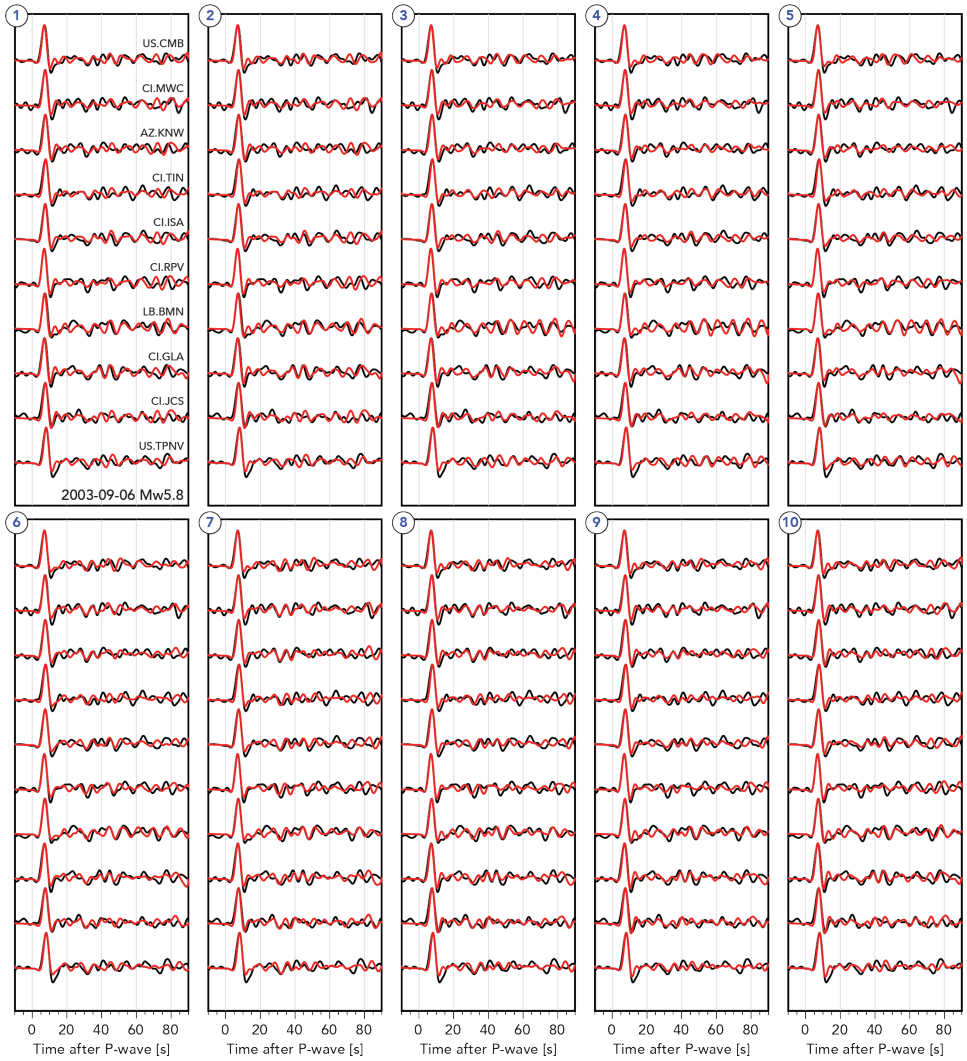


**Figure S9.** Waveform modeling results for the 2003 Mw5.8 event using the source locations in Figure S8. The depth of the sources is 5 km. Note that the wavefield shows little sensitivity to hypocentral location due to the fact that none of the sources are located in the immediate vicinity of the main fault or any other prominent bathymetric feature.

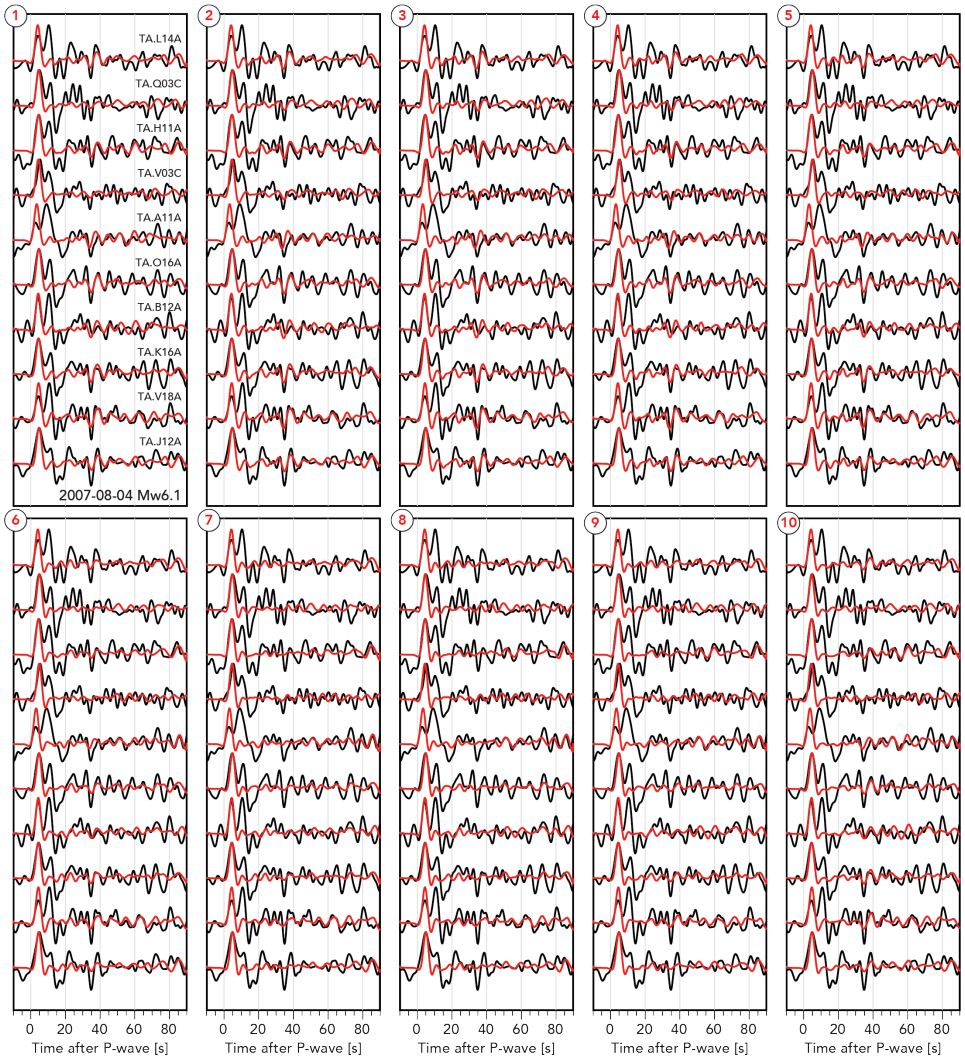


**Figure S10.** Waveform modeling results for the 2007 Mw6.2 event using the source locations in Figure S8. The depth of the sources is 5 km. Note that the wavefield shows high sensitivity to hypocentral location due to the fact that the sources are located in the immediate vicinity of the main fault.

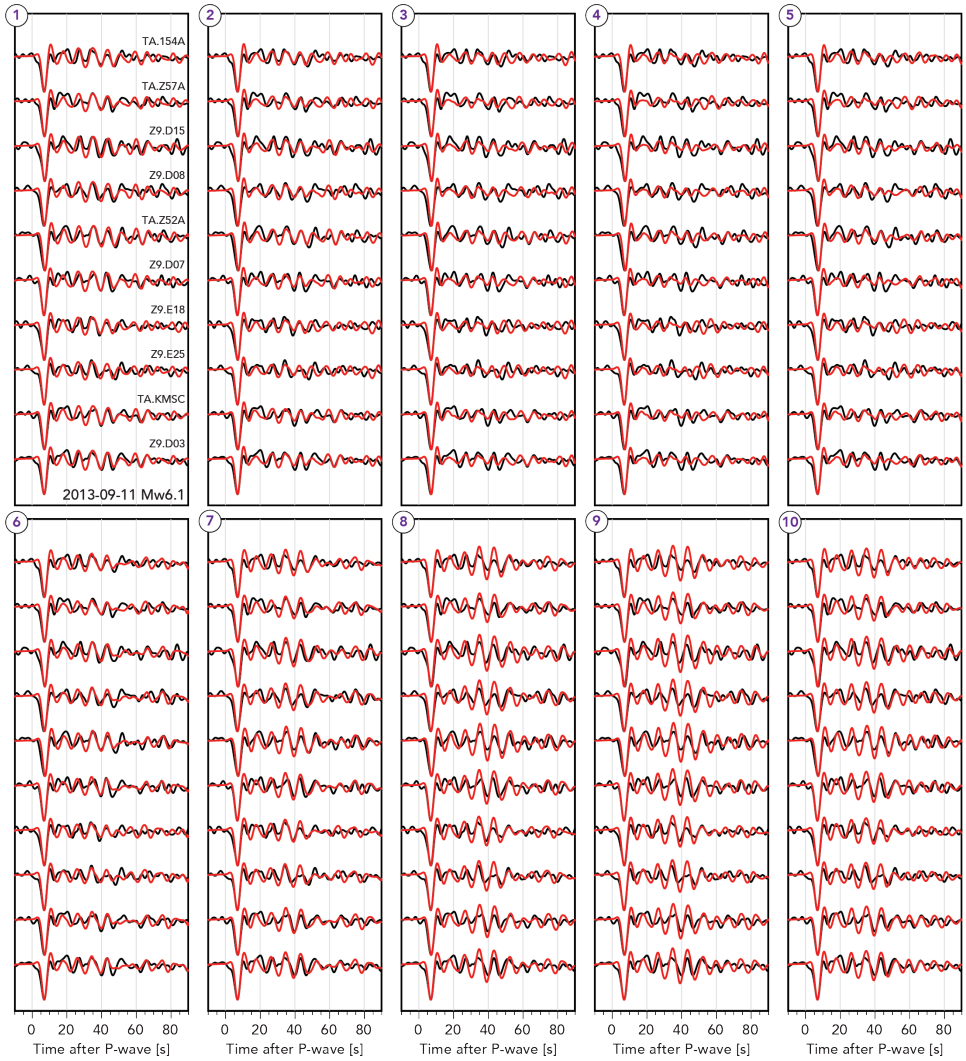


**Figure S11.** Waveform modeling results for the 2013 Mw6.1 event using the source locations in Figure S8. The depth of the sources is 5 km. Note that the wavefield shows little sensitivity to hypocentral location due to the fact that none of the sources are located in the immediate vicinity of the main fault or any other prominent bathymetric feature.

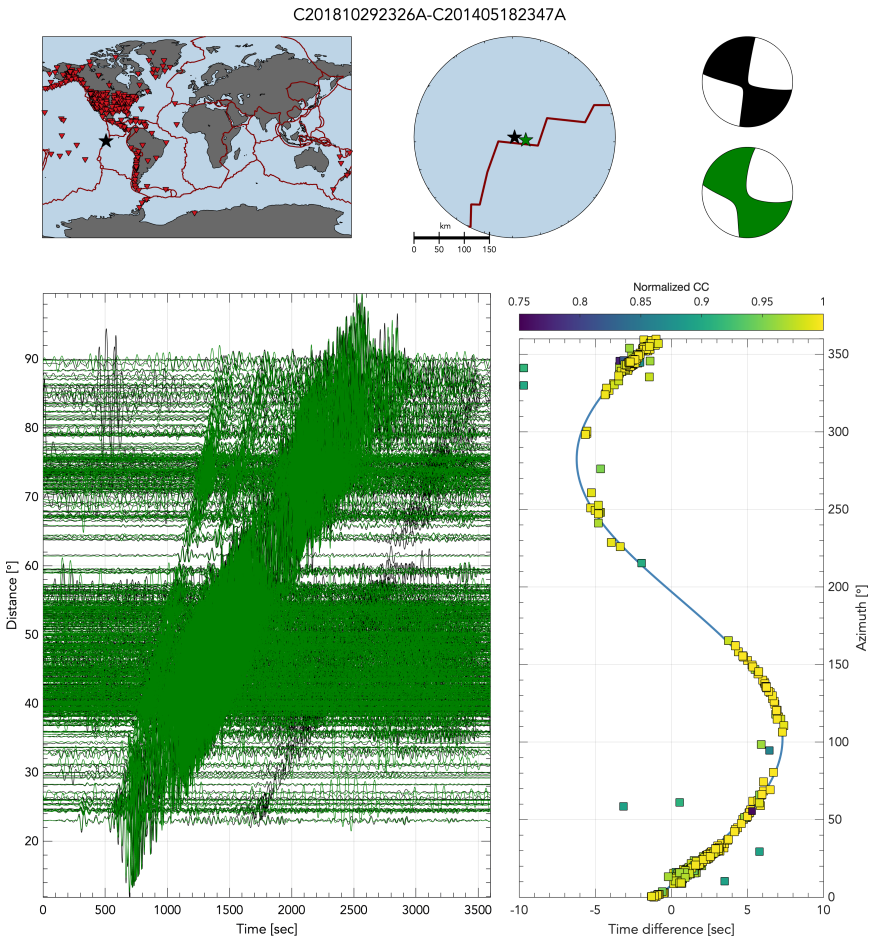


**Figure S12.** Surface wave time shift measurements for the 2018-10-29 Mw5.9 and 2014-05-18 Mw5.9 Gofar events. The top panels (from left to right) include a global map showing the station distribution (red inverted triangles), a regional map of the near-source site showing the GCMT location of the two events (black and green stars), and their respective focal mechanisms. The lower panels (from left to right) show the vertical component waveforms of the two events sorted by distance, and the observed time shifts for the two events as a function o azimuth. The waveforms have been band-passed between 30 and 80 seconds. The color of the markers indicate the normalized correlation coefficient between the two surface wave packets and the blue curve depicts the best fitting model. The black-colored star, focal mechanism, and traces correspond to the 2018 Mw5.9 event, whereas the green star, focal mechanism, and traces corresponds to the 2014 Mw5.9 event. The intersource distance estimated from this analysis gives a relative distance of 25 km.

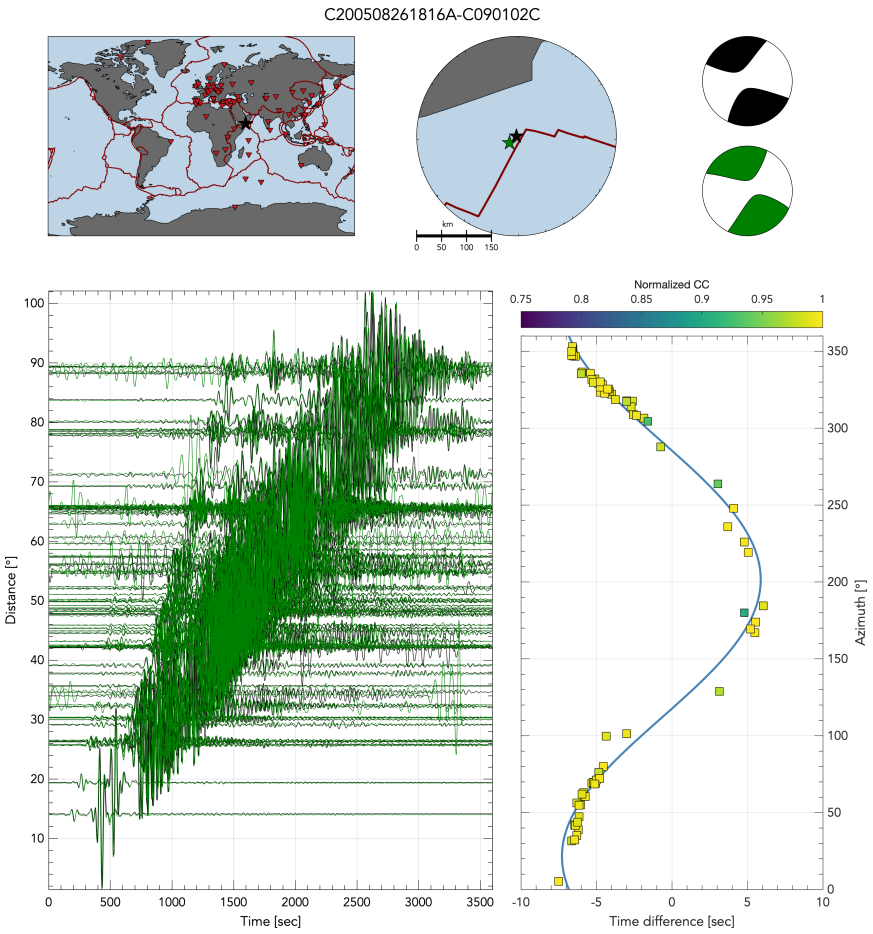


**Figure S13.** Surface wave time shift measurements for the 2005-08-26 Mw6.1 and 2002-09-01 Mw6.0 Alula Fartak events. The top panels (from left to right) include a global map showing the station distribution (red inverted triangles), a regional map of the near-source site showing the GCMT location of the two events (black and green stars), and their respective focal mechanisms. The lower panels (from left to right) show the vertical component waveforms of the two events sorted by distance, and the observed time shifts for the two events as a function o azimuth. The waveforms have been band-passed between 30 and 80 seconds. The color of the markers indicate the normalized correlation coefficient between the two surface wave packets and the blue curve depicts the best fitting model. The black-colored star, focal mechanism, and traces correspond to the 2005 Mw6.1 event, whereas the green star, focal mechanism, and traces corresponds to the 2002 Mw6.0 event. The intersource distance estimated from this analysis gives a relative distance of 26 km.